Proceedings of the 42nd IEEE
Conference on Decision and Control
Maui, Hawaii USA, December 2003

Visual Servoing of 6 DOF Manipulator by Multirate Control with Depth Identification

Hiroshi Fujimoto
Department of Electrical Engineering, Nagaoka University of Technology
Nagaoka, 940-2128 Japan, *hfuji@ieee.org*

***Abstract*— This paper presents a visual servoing of 6 degree-of-freedom (DOF) manipulator based on intersample disturbance rejection with switching scheme. In the controller, multirate intersample disturbance rejection algorithm is utilized, which was proposed by authors for general digital control system with restricted sampling frequency. The proposed feedforward scheme with open-loop estimation and switching function enables the disturbance rejection without any sacrifice of the closed-loop characteristics. A new precise formulation of delay problems in visual servoing is established as the image processing latency, the difference between sampling period of camera signal and control period of joint servo system, and delay of inner-loop joint servo system. By introducing novel multi-loop control schemes and depth identification, the proposed intersample disturbance rejection controller becomes applicable to the complicated visual servoing problem of 6 DOF manipulator with moving object points. Finally, the advantages of the proposed control system are verified through simulations using 6 DOF robot manipulator with multiple feature points.**

I. INTRODUCTION

Visual servoing plays very important role for robot manipulators to deal with objects in unknown environment. In the study of image-based visual servoing [1], recent important topics are 1) global instability on image-based method [2], 2) selection of features [3], and 3) problem about sensor latency. This paper deals with the 3rd topic by separating this latency into two problems. The first problem is that the vision sensor requires long time for image processing, and this delay works as dead-time to feedback control system. The second problem is that the sampling period of vision sensor such as a CCD camera is comparatively long (over 33 [ms]) while the control period of joint servo is short (less than 1 [ms]).

For the first problem of time delay modeled as e^{-sT_d}, many prediction methods such as Kalman filter [4], [5], AR model [6], $\alpha-\beta-\gamma$ filter [7], generalized predictive controller (GPC) [8], and nonlinear observer [9] have already been proposed. In this paper, the movement of object is modeled as output disturbance, and it is estimated and predicted by full-order disturbance observer.

For the second problem about difference between sampling period and control period which is expressed as $T_y > T_u$ in the notation of section II, several approaches have also been proposed based on interpolation [9], [10] and sampled-data optimal control [11]. Especially in [9], the intersample estimation method of object movement was proposed based on the motion model and its observer. However, these previous papers [4]–[11] simply deal with the delay as slow sensor problem, and they do not clearly distinguish the image processing delay (e^{-sT_d}) from the sampling period difference ($T_y > T_u$). On the other hand, this paper formulates this issue explicitly by establishing novel precise model of the delay problem. Moreover, this paper makes first attempt to reject the tracking error completely on image plane at intersample points.

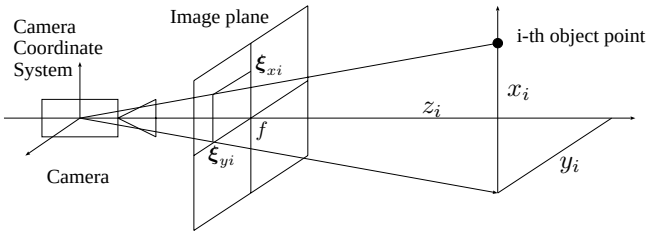

Fig. 1. Perspective model

In [12], authors applied the proposed intersample disturbance rejection to a simple visual servo system of 2 DOF manipulator with single feature point, and it was verified in experiments. This paper applies the intersample disturbance rejection algorithm to more general and complicated case of 6 DOF manipulator with multiple feature points by introducing new control schemes such as velocity screw controller in camera coordinates and depth identification method.

II. MODELING OF VISUAL SERVO SYSTEM

In this section, the visual servo problem is considered [1], in which the camera mounted on the robot manipulator tracks a moving object. Assume the m feature points are selected, and they are defined as $\boldsymbol{\xi} := [\boldsymbol{\xi}_1^T, \cdots, \boldsymbol{\xi}_m^T]^T$ and $\boldsymbol{\xi}_i := [\xi_{xi}, \xi_{yi}]^T (i = 1, \cdots, m)$. Let the positions and orientations of camera and object be $\boldsymbol{x}_c \in \boldsymbol{R}^6$ and $\boldsymbol{x}_o \in \boldsymbol{R}^6$, respectively. The camera is modeled by a mapping $\iota : \boldsymbol{R}^6 \times \boldsymbol{R}^6 \to \boldsymbol{R}^{2m}$ as

$$\boldsymbol{\xi} = \iota(\boldsymbol{x}_c, \boldsymbol{x}_o). \tag{1}$$

The derivative of (1) is calculated by

$$\dot{\boldsymbol{\xi}} = \frac{\partial \iota}{\partial \boldsymbol{x}_c}\dot{\boldsymbol{x}}_c + \frac{\partial \iota}{\partial \boldsymbol{x}_o}\dot{\boldsymbol{x}}_o \tag{2}$$

$$:= \boldsymbol{J}(\boldsymbol{\xi}, \boldsymbol{z})\boldsymbol{v}_c + \boldsymbol{d}_1(t) \tag{3}$$

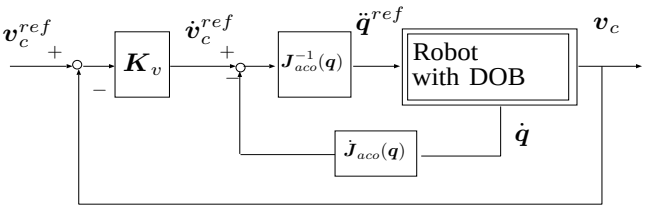

Fig. 2. Inner-loop velocity controller.

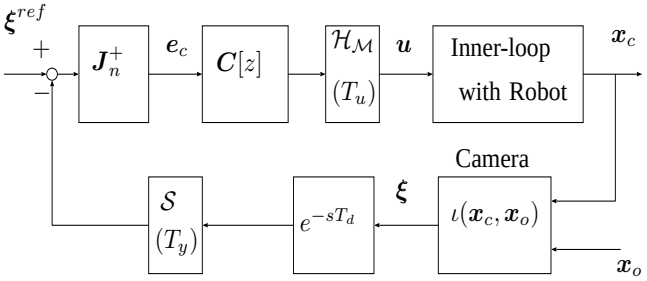

Fig. 3. Visual servo system.

where $\boldsymbol{J} := [\boldsymbol{J}_1^T, \cdots, \boldsymbol{J}_m^T]^T$ is the image Jacobian [1], $\boldsymbol{z} := [z_1, \cdots, z_m]^T$, z_i is the distance between the i–th object and camera shown in Fig. 1, $\boldsymbol{v}_c = \dot{\boldsymbol{x}}_c := [T_x, T_y, T_z, \omega_x, \omega_y, \omega_z]^T$ is the velocity screw of the camera frame expressed in the camera coordinates, $\boldsymbol{d}_1(t)$ is the disturbance caused by the motion of object, and $\boldsymbol{J}_i$ is defined as

$$\boldsymbol{J}_i := \begin{bmatrix} -\frac{f}{z_i} & 0 & \frac{\xi_{xi}}{z_i} & \frac{\xi_{xi}\xi_{yi}}{f} & -\frac{\xi_{xi}^2+f^2}{f} & \xi_{yi} \\ 0 & -\frac{f}{z_i} & \frac{\xi_{yi}}{z_i} & \frac{\xi_{yi}^2+f^2}{f} & -\frac{\xi_{xi}\xi_{yi}}{f} & -\xi_{xi} \end{bmatrix}, \quad (4)$$

where f is the focus distance.

By using the error of feature points, the controlled variable $\boldsymbol{e}_c$ is defined as

$$\boldsymbol{e}_c(t) := \boldsymbol{J}_n^+(\boldsymbol{\xi}^{ref} - \boldsymbol{\xi}(t)), \quad (5)$$

where $\boldsymbol{J}_n$ is the model of image Jacobian. In this paper, it is fixed to a constant matrix $\boldsymbol{J}_n := \boldsymbol{J}(\boldsymbol{\xi}^{ref}, \boldsymbol{z}_n)$ with the constant desired feature $\boldsymbol{\xi}^{ref}$ and nominal depth $\boldsymbol{z}_n$ in order to reduce the on-line calculation cost. The modeling error is defined as $\Delta := \boldsymbol{J}^+(\boldsymbol{\xi}, \boldsymbol{z}) - \boldsymbol{J}_n^+(\boldsymbol{\xi}^{ref}, \boldsymbol{z}_n)$. To guarantee the full rank of $\boldsymbol{J}$, the number of feature points is assumed to be $m \geq 4$ [3]. Thus, $\boldsymbol{J}_n^+$ is calculated by $\boldsymbol{J}_n^+ = (\boldsymbol{J}_n^T\boldsymbol{J}_n)^{-1}\boldsymbol{J}_n^T$. From (3), the derivative of (5) is given by

$$\dot{\boldsymbol{e}}_c(t) = -(\boldsymbol{J}^+ - \Delta)(\boldsymbol{J}\boldsymbol{v}_c(t) + \boldsymbol{d}_1(t)) \quad (6)$$
$$:= -\boldsymbol{v}_c(t) + \boldsymbol{d}_2(t) \quad (7)$$

where $\boldsymbol{d}_2(t) := \Delta(\boldsymbol{J}\boldsymbol{v}_c(t) + \boldsymbol{d}_1(t)) - \boldsymbol{J}^+\boldsymbol{d}_1(t)$.

III. Inner-loop controller design

In this section, the velocity controller is designed as inner-loop system in order to control the camera velocity $\boldsymbol{v}_c$, as shown in Fig. 2. While the workspace position controller is designed in the simple case of 2 DOF manipulator [12], the velocity screw should be controlled in the camera coordinates to obtain linear diagonal plant of the 6 DOF system.

Because this inner-loop controller employs the robust disturbance observer (DOB) in the joint space, it is possible to assume that each joint axis is decoupled under the cut-off frequency of DOB [13]. Therefore, if the non-singularity of Jacobian $\boldsymbol{J}_{aco}$ is assured, the transfer function from the acceleration command $\dot{\boldsymbol{v}}_c^{ref}$ to the velocity $\boldsymbol{v}_c$ can be regarded as a integrator system in the frequency region below the cut-off frequency [13]. In this 6 DOF manipulator case, $\boldsymbol{J}_{aco}$ is the manipulator Jacobian in camera coordinates.

Because this inner-loop controller needs only encoder information as sensor output, the sampling time can be set very shortly compared with outer-loop visual controller which requires camera information. The typical sampling time of inner-loop system is 0.2 $\sim$ 1 [ms], and the typical cut-off frequency of DOB is 150 $\sim$ 300 [rad/s] [12], [13].

If the velocity controller $\boldsymbol{K}_v$ is simply selected as diagonal gain matrix $\boldsymbol{K}_v = \mathrm{diag}\{K_v, \cdots, K_v\}$, the inner-loop system can be expressed in the frequency region below the cut-off frequency of DOB as

$$\boldsymbol{v}_c(s) = \frac{K_v}{s + K_v}\boldsymbol{I}_6\boldsymbol{u}(s), \quad (8)$$

where the velocity reference $\boldsymbol{v}_c^{ref}$ is selected as the control input from the outer-loop visual servo controller ($\boldsymbol{u} = \boldsymbol{v}_c^{ref}$). Because the cut-off frequency of DOB is much higher than the target frequency region of the outer-loop system, this model (8) is very good approximation in the design of the visual servo controller.

IV. Outer-loop controller design

From (8), the Laplace transformation of (7) is given by

$$\boldsymbol{e}_c(s) = -\frac{\boldsymbol{v}_c(s)}{s} + \frac{\boldsymbol{d}_2(s) + \boldsymbol{e}_c(t=0)}{s} \quad (9)$$
$$= \boldsymbol{P}(s)\boldsymbol{u}(s) + \boldsymbol{d}(s). \quad (10)$$

where $\boldsymbol{P}(s) = -\frac{K_v}{s(s+K_v)}\boldsymbol{I}_6$ and $\boldsymbol{d}(s) = \frac{\boldsymbol{d}_2(s)+\boldsymbol{e}_c(t=0)}{s}$.

Because the linear diagonal plant model $\boldsymbol{P}(s)$ is obtained, the multirate controller proposed in [12] is applicable and it can be implemented as shown in Fig. 3. Thus, the controllers can be designed independently in each axis of $\boldsymbol{v}_c(= [T_x, T_y, T_z, \omega_x, \omega_y, \omega_z]^T)$. Since the movement of the object is expressed as $\boldsymbol{d}_1(t)$, it can be regarded as the output disturbance $\boldsymbol{d}(t)$ in (9). Therefore, the proposed method can achieve high tracking performance.

In the intersample disturbance rejection which was proposed by authors in [12], the disturbance is modeled as

$$\dot{\boldsymbol{x}}_d(t) = \boldsymbol{A}_{cd}\boldsymbol{x}_d(t), \ d(t) = \boldsymbol{c}_{cd}\boldsymbol{x}_d(t), \quad (11)$$

where $\boldsymbol{A}_{cd}$ and $\boldsymbol{c}_{cd}$ are known parameters, and $\boldsymbol{x}_d(t)$ is unknown state variable. For example, the step-type disturbance with unknown amplitude can be modeled by $\boldsymbol{A}_{cd} = 0, \boldsymbol{c}_{cd} =$

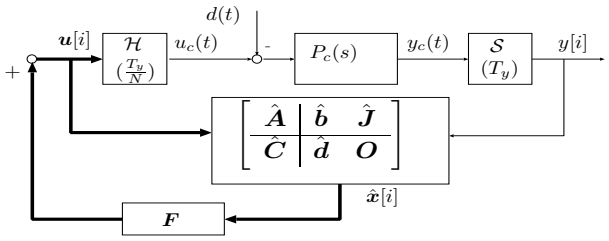

Fig. 4. Feedback disturbance rejection.

1, and sinusoidal type disturbance with known frequency ω_d and unknown amplitude and phase can be modeled by

$$\boldsymbol{A}_{cd} = \boldsymbol{A}_{\omega}(\omega_d) := \begin{bmatrix} 0 & 1 \\ -\omega_d^2 & 0 \end{bmatrix}, \quad \boldsymbol{c}_{cd} = [1, 0]. \quad (12)$$

The disturbance model (11) covers wide class of typical object movement such as constant velocity motion, constant acceleration motion, parabolic motion, circular motion, and repetitive motion. Moreover, the motion unknown parameters $\boldsymbol{x}_d(t)$ are allowed to be changed during the motion because the observer estimates $\boldsymbol{x}_d(t)$ in real-time. For instance, in the constant velocity motion which is modeled by (12) with $\omega_d = 0$, the initial position and velocity are represented as $\boldsymbol{x}_d(0) \in \boldsymbol{R}^2$. If the velocity is suddenly changed, it can be estimated immediately by the observer. Moreover, if some parameters in $\boldsymbol{A}_{cd}$ and $\boldsymbol{c}_{cd}$ are unknown, they can be adaptively identified by nonlinear observer [9].

In Fig. 3, T_y is the sampling period of camera, $T_u := T_y/N$ is the control period to inner-loop, and e^{-sT_d} represents time delay caused by image processing, which normally requires one sampling time ($T_d = T_y$). Because this delay generates difficulty in feedback system, the full order observer is utilized in order to predict one-step ahead state variable and compensate the time delay. Moreover, the proposed intersample disturbance rejection is assured not only for the one sampling-time delay but also for the non-integer sampling-time delay [12].

V. Simulations of FB disturbance rejection

In this section, the feedback disturbance rejection (Fig. 4) proposed in [12] is verified through simulation. The vertices of a square 40 centimeters on a side are selected as feature points ($m = 4$). Fig. 5 shows the initial poses of 6 DOF manipulator of puma 560 and the object. The object points are moved on circles in y-z plane at $x = 2$[m] with angular velocity $f_{obj} = 0.5$ [Hz] as shown Fig. 10. The simulation is performed by MATLAB/Simulink with Robotics Toolbox [14]. This Toolbox offers useful functions such as kinematics, dynamics, and camera model, and it enables us to check the motions both of manipulator and image features through animation. The camera parameters are shown in Table I[1].

[1]The simulation conditions such as camera parameters and object size are decided to refer the visual servoing example in Robotics Toolbox [14].

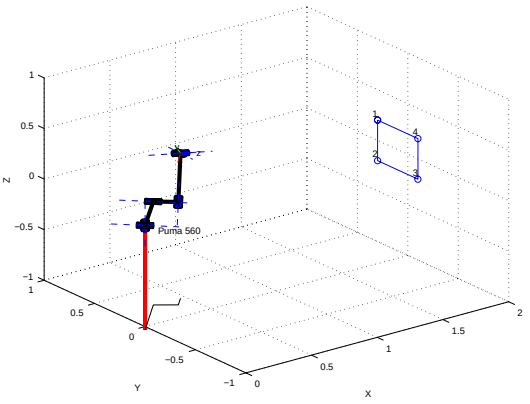

Fig. 5. Initial pose.

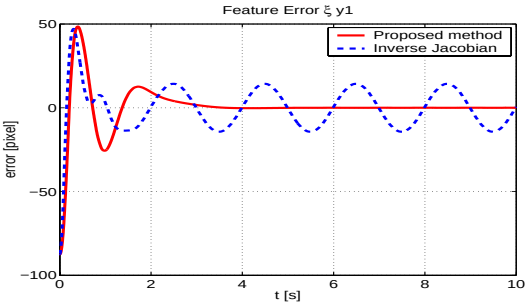

Fig. 6. Feature error (Multi-rate vs. Inverse Jacobian).

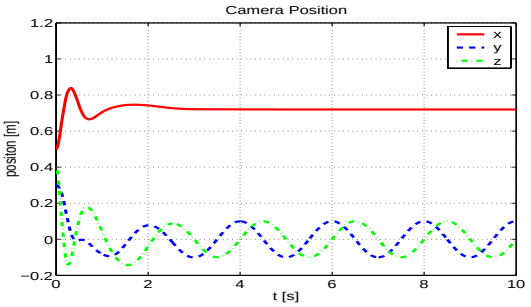

Fig. 7. Camera position.

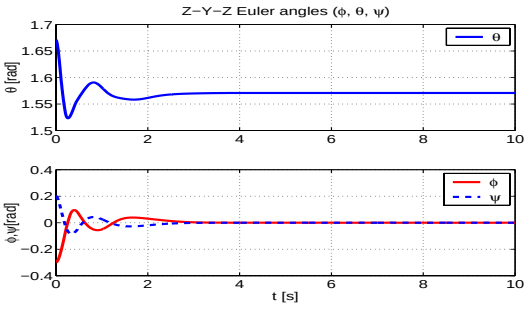

Fig. 8. Camera orientation.

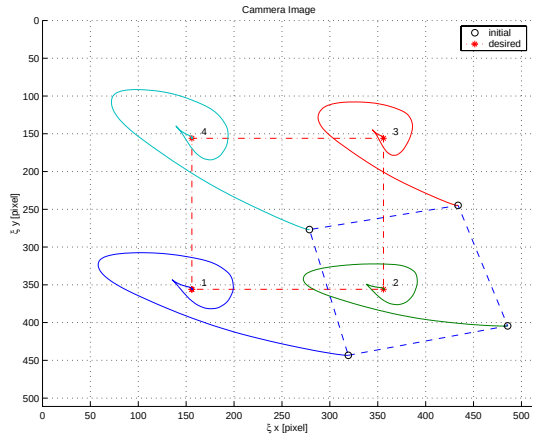

Fig. 9. Image feature trajectories.

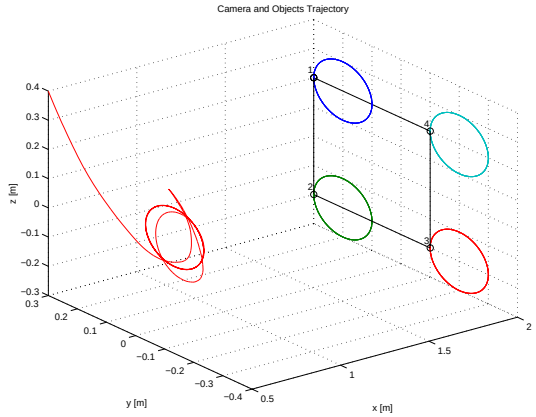

Fig. 10. Camera and objects trajectories.

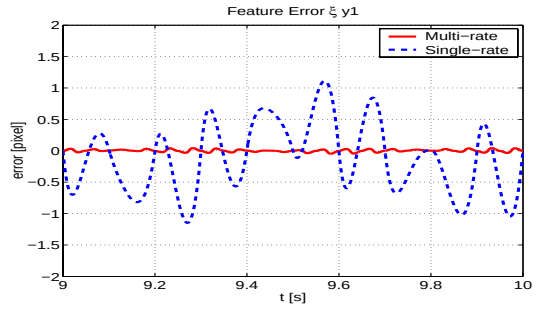

Fig. 11. Feature error (Multi-rate vs. Single-rate).

TABLE I

CAMERA PARAMETERS IN SIMULATIONS.

dimension	512 × 512 [pixel]
focus length	8 [mm]
pixel pitch	80,000 [pixel/m]
center point	(256, 256) [pixel]

The sampling period of the image and the control period of the velocity command $\boldsymbol{v}_c^{ref}$ are set to $T_y = 100$ [ms] and $T_u = 25$ [ms], respectively[2]. Because the input multiplicity is $N = 4$ and the order of plant (9) is $n = 2$, perfect disturbance rejection is assured at $2(= N/n)$ intersample points [12].

The multirate feedback controller is designed with step and $f_{obj} = 0.5$ [Hz] sinusoidal disturbance model $\boldsymbol{A}_{cd} = \mathrm{diag}\{0, \boldsymbol{A}_\omega(2\pi f_{obj})\}$ because $\boldsymbol{d}_1$ has strong spectrum at f_{obj} and $\boldsymbol{d}(s)$ has $1/s$ in (9). Fig. 6 shows the comparison results between the proposed method and well-known inverse image Jacobian method, in which the control law is described as $\boldsymbol{v}_c^{ref}[i] = \gamma \boldsymbol{J}^+(\boldsymbol{\xi}[i], \boldsymbol{z}_n)(\boldsymbol{\xi}^{ref} - \boldsymbol{\xi}[i])$. The gain γ is tuned to minimize the steady-state error and $\gamma = 10$ is obtained. While the inverse Jacobian method has large steady-state error caused by object movement, the proposed method converges to zero feature error.

Fig. 7 and 8 show the camera pose of the proposed method. It is shown that the camera approaches toward the object in x-direction and moves on circle in y, z-direction to obtain the desired feature. While the initial orientation is given as $(\phi, \theta, \psi) = (-0.3, \pi/2 + 0.1, 0.2)$ in Z-Y-Z Euler angles, it successfully converges to $(0, \pi/2, 0)$ by the proposed scheme.

While the nominal depth is given by $\boldsymbol{z}_n = [1.5, \cdots, 1.5]^T$, the true value is $\boldsymbol{z} = [1.28, \cdots, 1.28]^T$ at the steady-state. Although the modeling error Δ is generated by the depth mismatch even in the steady-state, the feature error converges to zero as shown in Fig. 6 and Fig. 11. The convergence is theoretically assured by internal model principle because the controller has the disturbance model of $\boldsymbol{A}_\omega(2\pi f_{obj})$ in the case of FB disturbance rejection.

Fig. 9 and 10 show the trajectories of image feature points and camera position. Because the image Jacobian is fixed to the constant matrix $\boldsymbol{J}_n$ in the control law, the trajectories overshoot the desired points against the moving object. In spite of that, the features converge to desired image points in steady-state.

Fig. 11 shows the comparison results of steady-state feature error between the proposed multirate control and conventional single-rate control with the same disturbance model. In Fig. 11, the object speed is set to faster value $f_{obj} = 1.5$[Hz] to show the difference clearly. Although the feature error becomes zero at every sampling point ($T_s = 0.1$[s]), the inter-sample error of single-rate system is larger than the multirate system. On the other hand, in the proposed method, the error $\boldsymbol{e}_c(t)$ and its derivative $\dot{\boldsymbol{e}}_c(t)$ are regulated to zero at $M(= 2)$ intersample points because the plant state is selected as $\boldsymbol{x}_p = [\boldsymbol{e}_c, \dot{\boldsymbol{e}}_c]^T$.

[2]The sampling time 100 [ms] is set to be longer than the normal video-rate 33 [ms] so that the inter-sample response can be evaluated in the future experiments.

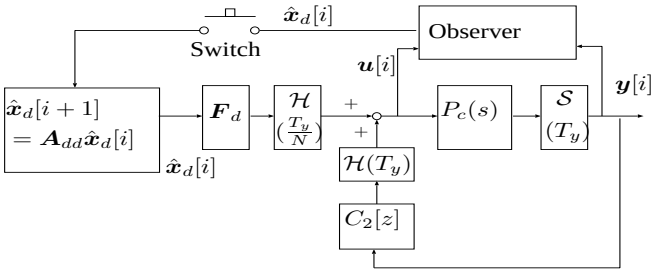

Fig. 12. Feedforward disturbance rejection.

VI. Simulations of FF disturbance rejection

In this section, the feedforward disturbance rejection of Fig. 12 [12] is verified for the high speed movement of $f_{obj} = 1.5$[Hz]. In this scheme, the disturbance state variable in (11) is estimated by the open-loop disturbance observer. When the estimation converges to the steady state, the switch turns on at $t = t_0$. After that, the switch turns off immediately. The disturbance can be calculated by the model from the initial value $\hat{\boldsymbol{x}}_d[t_0]$. The disturbance feedforward $\boldsymbol{F}_d$ obtained from [12] guarantees perfect intersample disturbance rejection at M inter-sample points.

Fig. 13 shows the sensitivity and complementary sensitivity functions $S[z]$ and $T[z]$ both of the feedback (Fig. 4) and the feedforward (Fig. 12) disturbance rejection control. Fig. 13(a) indicates the disadvantages of the feedback approach, where the closed-loop characteristics worsen and it becomes difficult to assure stability robustness. On the other hand, in the proposed feedforward approach (Fig. 12), the closed-loop characteristics depend only on $\boldsymbol{C}_2[z]$ which does not need to have the internal model of disturbance. Therefore, the feedback characteristics are better than those of the feedback approach.

However, the performance robustness of feedforward disturbance rejection is determined by the feedback controller $\boldsymbol{C}_2[z]$. Because the variation of feedforward performance under the variation of plant is decided by sensitivity function $\boldsymbol{S}[z]$, the robustness of disturbance rejection performance depends on $\boldsymbol{C}_2[z]$. Thus, if the disturbance frequency is over the cut-off frequency of $\boldsymbol{S}[z]$, the performance is worsen by plant variation.

Fig. 14 shows the simulation results for high speed object $f_{obj} = 1.5$[Hz] with the constant nominal depth $\boldsymbol{z}_n = [1.5, \cdots, 1.5]^T$. Because the image Jacobian is fixed to constant matrix $\boldsymbol{J}(\boldsymbol{\xi}^{ref}, \boldsymbol{z}_n)$, the depth mismatch causes the plant variation Δ even in the steady-state. Moreover, the disturbance frequency 1.5[Hz] is much higher than the cut-off frequency of $\boldsymbol{S}[z]$, as shown in Fig. 13(b). Thus, Fig. 14 has steady-state error after the switching-time $t_0 = 5$[s].

Therefore, the depth information is estimated by recursive least-squares (RLS) algorithm [15]. From (3), the regression model of unknown parameter $\theta_i := \frac{1}{z_i}$ $(i = 1, \cdots, m)$ is

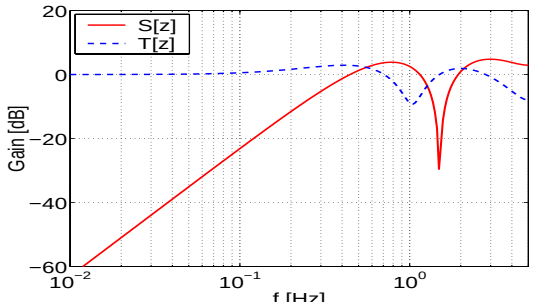

(a) Feedback

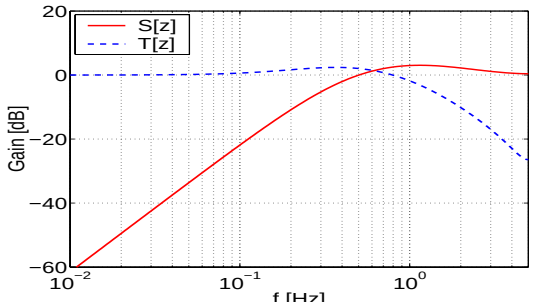

(b) Feedforward

Fig. 13. Frequency responses ($S[z]$ and $T[z]$).

obtained by

$$\boldsymbol{y}_i = \boldsymbol{\varphi}_i^T \theta_i + \boldsymbol{d}_{1i}, \tag{13}$$

where

$$\boldsymbol{y}_i := \begin{bmatrix} \dot{\xi}_{xi} \\ \dot{\xi}_{yi} \end{bmatrix} - \begin{bmatrix} \frac{\xi_{xi}\xi_{yi}}{f}\omega_x - \frac{\xi_{xi}^2+f^2}{f}\omega_y + \xi_{yi}\omega_z \\ \frac{\xi_{yi}^2+f^2}{f}\omega_x - \frac{\xi_{xi}\xi_{yi}}{f}\omega_y - \xi_{xi}\omega_z \end{bmatrix}, \tag{14}$$

$$\boldsymbol{\varphi}_i^T := \begin{bmatrix} -fT_x + \xi_{xi}T_z \\ -fT_y + \xi_{yi}T_z \end{bmatrix}. \tag{15}$$

Fig. 15 shows the estimated depth $\hat{z}_1$. The implemented algorithm is RLS with exponential forgetting and conditional updating [16]. To remove the disturbance effect, the both signals of y_i and φ_i are filtered by band blocking filter. The updating condition is selected as $\boldsymbol{\varphi}_i\boldsymbol{\varphi}_i^T > \epsilon(:= 10^{-10})$. Because this condition is not satisfied after $t = 3.5$[s], the estimation update is stopped to avoid the divergence of estimator state by the poor persistent excitation (PE).

Fig. 16 shows the feature error of feedforward disturbance rejection with estimated depth. The depth $\boldsymbol{z}$ in $\boldsymbol{J}_n^+$ is switched from the nominal value 1.5 to estimated value at $t = 4$[s]. The high frequency disturbance is rejected completely after the switching time $t_0 = 5$[s].

By above discussion, the problem of the proposed feedforward disturbance rejection is founded, and it is overcome by adaptive scheme. Next, the advantage of this method is mentioned. Fig. 17 shows the x-axis camera position in world coordinates which corresponds the T_z direction of camera coordinates in the steady-state. While the transient

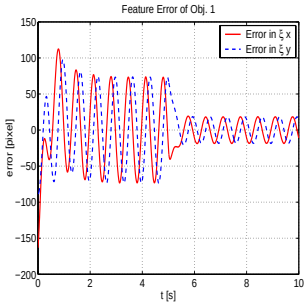

Fig. 14. Feature error without depth estimation.

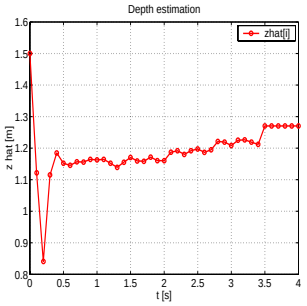

Fig. 15. Estimated depth $\hat{z}_1$. (RLS with conditional updating)

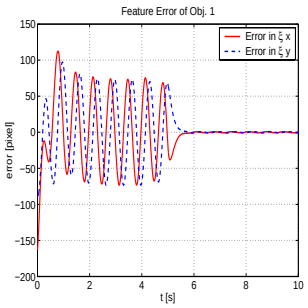

Fig. 16. Feature error with depth estimation.

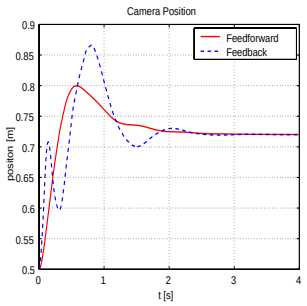

Fig. 17. Camera position X_c (Feedforward vs. Feedback)

response of FB disturbance rejection is oscillated by the high frequency internal model shown in Fig. 13(a), that of the FF method is smooth and stable. Moreover, the FB method could become unstable when many disturbance components are considered [17]. On the other hand, the FF method can preserve the good stability robustness.

VII. Conclusion

In this paper, novel multirate controller was applied to the visual servo system of 6 DOF manipulator. Because the proposed control system assured the perfect disturbance rejection at M intersample points, the control system achieved high tracking performance.

The advantages and drawbacks both of feedback and feedforward disturbance rejection algorithm were demonstrated. The feedback approach has strong robust performance against the plant uncertainty because of the internal model principle. However, the internal model of high frequency disturbance damages the closed-loop characteristics, which causes poor stability robustness. On the other hand, the feedforward approach preserves the excellent closed-loop characteristics and stability robustness. However, if the disturbance components is over the closed-loop cut-off frequency, the adaptive scheme is required to reduce the modeling error.

Because this method is based on inverse Jacobian $\boldsymbol{J}_n^+$, the global stability is not assured as pointed out in [2]. In order to assure the global stability, specific approach such as [18] and [19] should be combined into the proposed method. It will be one of the future works.

However, this paper established new formulation of the delay problems in visual servoing as the difference between T_y and T_u, the image processing delay e^{-sT_d}, and inner-loop delay $\boldsymbol{P}(s)$. Moreover, the novel control methods were proposed to overcome these problems. Finally, the author would like to note that part of this research is carried out with a subsidy of the FANUC FA and Robot Foundation.

VIII. References

[1] S. Hutchinson, G. D. Hager and P. I. Corke: “A tutorial on visual servo control”, IEEE Trans. Robotics and Automation, **12**, 5, pp. 3745–3750 (1996).

[2] F. Chaumette: “Potential problems of stability and convergence in image-based and position-based visual servoing”, The Confluence of Vision and Control, **237**, pp. 66–78 (1998).

[3] K. Hashimoto and T. Noritsugu: “Performance and sensitivity in visual servoing”, IEEE Int. Conf. Robotics and Automation, pp. 2321–2326 (1998).

[4] F. Chaumette and A. Santos: “Tracking a moving object by visual servoing”, IFAC World Congress, Vol. 9, pp. 409–414 (1993).

[5] P. I. Corke and M. C. Good: “Dynamics effects in visual closed-loop systems”, IEEE Trans. Robotics and Automation, **12**, 5, pp. 671–683 (1996).

[6] A. J. Koivo and N. Houshangi: “Real-time vision feedback for servoing robotic manipulator with self-tuning controller”, IEEE Trans. Systems, Man, and Cybernetics, **21**, 1, pp. 134–142 (1991).

[7] P. K. Allen, A. Timcenko, B. Yoshimi and P. Michelman: “Automated tracking and grasping of a moving object with a robot hand-eye system”, IEEE Trans. Robotics and Automation, **9**, 2, pp. 152–165 (1993).

[8] J. A. Gangloff, M. Mathelin and G. Abba: “6 DOF high speed dynamic visual servoing using GPC controllers”, IEEE Int. Conf. Robotics and Automation, pp. 2008–2013 (1998).

[9] K. Hashimoto and H. Kimura: “Visual servoing with nonlinear observer”, IEEE Int. Conf. Robotics and Automation, pp. 484–489 (1995).

[10] J. T. Feeddma and O. R. Mitchell: “Vision guided servoing with feature-based trajectory generation”, IEEE Trans. Robotics and Automation, **5**, 5, pp. 691–700 (1989).

[11] M. Nemani, T. C. Tsao and S. Hutchinson: “Multi-rate analysis and design of visual feedback digital servo-control system”, ASME, J. Dynam. Syst., Measur., and Contr., **116**, pp. 44–55 (1994).

[12] H. Fujimoto and Y. Hori: “Visual servoing based on intersample disturbance rejection by multirate sampling control – time delay compensation and experimental verification –”, Conf. Decision Contr., pp. 334–339 (2001).

[13] T. Murakami, N. Oda, Y. Miyasaka and K. Ohnishi: “A motion control strategy based on equivalent mass matrix in multidegree-of-freedom manipulator”, IEEE Trans. Industrial Electronics, **42**, 2, pp. 259–265 (1995).

[14] P. I. Corke: “A robotics toolbox for MATLAB”, IEEE Robotics and Automation Magazine, **3**, 1, pp. 24–32 (1996).

[15] N. P. Papanikolopoulos and P. K. Khosla: “Adaptive robotic visual tracking: theory and experiments”, IEEE Trans. Automat. Contr., **38**, 3, pp. 429–445 (1993).

[16] K. J. Åström and B. Wittenmark: “Adaptive Control”, Addison-Wesley Publishing Company (1995).

[17] H. Fujimoto, F. Kawakami and S. Kondo: “Multirate repetitive control and applications – verification of switching scheme by HDD and visual servoing –”, Amer. Control Conf., pp. 2875–2880 (2003).

[18] P. I. Corke and S. Hutchinson: “A new hybrid image-based visual servo scheme”, Conf. Decision Contr., pp. 2521–2526 (2000).

[19] K. Hashimoto and T. Noritsugu: “Enlargement of stable region in visual servo”, Conf. Decision Contr., pp. 3927–3932 (2000).